Figure 1—figure supplement 1. Transcript changes elicited by WINi in MLLr cancer cells. (**A**) Crystal structures of C6 or C16 bound to the WIN Site of WDR5 with electrostatic surfaces mapped [PDB IDs: 6E23 (Aho et al., 2019a); 6UCS (Tian et al., 2020)]. (**B**) Viabilities of MV4;11 cells treated with a serial dilution range of either C6 (left) or C16 (right) for 72 hours, relative to viability of DMSO-treated cells (*n* = 3; Mean ± SEM). (**C**) As in (B) but for MOLM13 cells. (**D**) Transcript levels as determined by QuantiGene™ analysis of representative WDR5-bound (color) or non-bound (grayscale) ribosomal protein genes in MOLM13 cells treated with a serial dilution range of either C6 (left) or C16 (right) and relative to DMSO-treated cells (*n* = 3; Mean ± SEM). Vertical dashed line indicates either 2 μM C6 (left) or 100 nM C16 (right). (**E**) Transformed z-scores of genes with significantly altered transcript levels (RNA-Seq) in MV4;11 cells treated with either C6 (2 μM) or C16 (100 nM) for 48 hours, compared to DMSO-treatment. (**F**) Volcano plots, showing transcript level alterations in MV4;11 cells treated 48 hours with 2 μM C6 (left) or 100 nM C16 (right) compared to DMSO (*n* = 3; red indicates FDR < 0.05). (**G**) Dispersion plot describing the variance in gene expression for the RNA-seq data in a previous study (left) and this study (right).

Figure 1—figure supplement 2. Impact of WINi on *RPL22L1* and p53 target gene expression. (**A**) Venn diagram, showing the overlap of consensus p53 target genes (Fischer, 2017) with genes significantly induced by C6 or C16 in MV4;11 cells. (**B**) Graph showing the change in expression of the

91common genes in (A) elicited by WIN site inhibitor (WINi) C6 (red) or C16 (blue) in MV4;11 cells, compared to DMSO. (**C**) Changes in expression (and FDR) of *RPL22L1* elicited in response to C6 (red) or C16 (blue) treatment of K562 leukemia cells (Aho et al., 2019a) or five rhabdoid tumor cell lines [TTC642, KYM-1, G401, TM87-16, and TTC549; (Florian et al., 2022)].

Figure 2—figure supplement 1. WINi suppress translation. (**A**) Distribution of ribosome protected fragment (RPF) lengths in each Ribo-Seq sample/replicate. The length distribution of RPF in mammalian Ribo-Seq experiments typically peaks at 30–31 nucleotides. (**B**) Proportion of RPFs mapping to the coding sequence (CDS) or 5' or 3' untranslated regions (UTR) of transcripts. Color of dots is the same as in (A). (**C**) Proportion of RPFs mapping to each reading frame in the 5' UTR (left), the CDS (middle), and the 3' UTR. Color of dots is the same as in (A). (**D**) Magnitudes of significant TE alterations of mRNAs in each quartile (stratified by TE in DMSO) in cells treated with C6 (left) or C16 (right). Color dots represent individual genes. Bottom, middle, and top horizontal lines of each box represent first, second, and third quartiles, respectively. Vertical lines extend to data points within 1.5-fold of the interquartile range. Black dots represent values beyond 1.5-fold of the inter-quartile range.

(**E**) Changes in TE induced by C6 (left) or C16 (right) in MV4;11 cells, binned according to mRNA TOPscores (Philippe et al., 2020). Dashed lines represent the median; dotted lines indicate quartiles. Significance by t-test is indicated compared to group with TOPscore 0 to 1 ('*' ≤ 0.05, '**" ≤ 0.0001). (**F**) UpSet plot, showing the breakdown of genes encoding PRMT5 substrates (Radzisheuskaya et al., 2019) whose transcript levels and/or translation efficiencies decrease following WIN site inhibition (*p*-value calculated by hypergeometric test for over-representation of genes encoding PRMT5 substrates in genes with decreased translation efficiencies). (**G**) Overlap of C6/C16 common mRNAs with decreased abundance (RNA; blue) and those with decreased translation efficiency (TE; salmon), grouped according to the indicated Hallmark.MSigDB categories. (**H**) Overlap of all C6/C16 common mRNAs with altered abundance and decreased TE. (**I**) The top row of the heatmap displays the codon stability coefficient (CSC) for each codon (Wu et al., 2019) ranked from lowest ('Non-optimal') to highest ('Optimal'). The middle row displays enrichment of each codon in mRNAs that are decreased at both the TE and mRNA levels (RNA+TE) versus those that show a decrease in TE without an accompanying decreased in mRNA abundance (TE only). Bottom row is -Log10 FDR.

Figure 2—figure supplement 2. WINi impair translation of mitochondrial ribosomal proteins. (**A**) Top: Transcript level changes in mitochondrial ribosomal protein genes elicited by C6 or C16, as indicated. Bottom: Translational efficiency (TE) changes in mitochondrial ribosomal protein genes elicited by C6 or C16. All of the mitochondrial RPGs are nuclear-encoded; none have detectable binding of WDR5.

Figure 3—figure supplement 1. Enrichment analysis of proteins with altered expression in response to C16 treatment. (**A**) Graphs showing enrichment of proteins in GO BP (top) and Hallmark.MSigDB (bottom) pathways that are induced by C16 treatment at 24 (blue) or 72 (green) hours. The x-axis displays -Log10 (FDR); the number of proteins in each category is given in italics. (**B**) Graphs showing enrichment of proteins in GO BP (top) and Hallmark.MSigDB (bottom) pathways that are suppressed by C16 treatment at 24 (red) or 72 (brown) hours. The x-axis displays -Log10 (FDR); the number of proteins in each category is given in italics. See **Figure 3—source data 2** for output of the full enrichment analyses.

Figure 4—figure supplement 1. Genome wide CRISPR screen identifies genes that influence response to C6/C16. (**A**) Tier 1 screen: Daily cell counts of MV4;11 Cas9 and MV4;11 Cas9 + GeCKOv2 (Library) populations treated with either DMSO or 2 μM C6. The two replicates of this screen are shown separately. (**B**) Normalized counts of each sgRNA (x-axis) in the GeCKOv.2 library targeting *TP53* in the initial transduced cells (red; not visible on this scale) and the C6-treated population (blue). Data represents means of replicates; **"*"** indicates FDR < 0.05. (**C**) As in (B) but for sgRNAs targeting

CDKN2A. (**D**) Schematic of the *CDKN2A* gene locus with indicated sites complementary to Tier 1 and Tier 2 screen sgRNAs. Red sgRNAs increase in representation in CRISPR screens. (**E**) miRNet 2.0 (Chang & Xia, 2023) analysis of the 27 miRNAs enriched in the Tier 1 screen produced a single significant hit corresponding to the KEGG p53 signaling pathway. The miRNAs are represented as blue boxes and target genes as red circles; the connections between them are indicated. (**F**) As in (B) but for sgRNAs targeting *RPL22*. (**G**) Volcano plots, showing gene-level changes from the Tier 2 screen in sgRNA representation in C6- (left) and C16- (right) treated populations compared to DMSO control cultures (orange indicates FDR < 0.05). (**H**) Graph depicting gene-level Log2 FC and FDR values for genes that were flagged as C6- (squares) or C16- (circles) specific in the Tier 2 screen. (**I**) GO enrichment analysis of the 57 C6/C16 common genes emerging from Tier 2 of the screen. Italics represent the number of genes in each category. (**J**) Western blot analysis of γ-H2A.X (top) or H2A.X (bottom) levels in MV4;11 cells treated for three days with the indicated dose of C16. Etoposide ("Etop.") treatment was used as a positive control. GAPDH is a loading control. Representative images from three biological replicates shown. Raw unprocessed gel images for the data in (J) are presented in **Figure 4—source data 3**.

Figure 5—figure supplement 1. C16 is synergistic with multiple agents in MV4;11 cells. (**A**) Heatmaps of MV4;11 cell growth inhibition at each dose of C16 and the indicated five compounds. (**B**) Heatmaps of δ scores from MV4;11 cells at each dose combination of C16 and the indicated agents.

Figure 5—figure supplement 2. C16 is synergistic with multiple agents in MOLM13 cells. (**A**) Heatmaps of MOLM13 cell growth inhibition at each dose of C16 and the indicated five compounds. (**B**) Heatmaps of δ scores from MOLM13 cells at each dose combination of C16 and the indicated agents.

Figure 5—figure supplement 3. Impact of C16 and mivebresib on RPG and p53 target gene expression. (**A**) Transcript level changes in WDR5-bound (left) and non-bound (right) RPGs elicited by C16 (top), mivebresib (Mivb; middle) or the combination (bottom). (**B**) Heatmap, showing significant changes in the expression of consensus p53 target genes (Fischer, 2017) induced by C16, mivebresib (Mivb; middle) or the combination (bottom) in MV4;11 cells.

Figure 6—figure supplement 1. WINi alter the abundance of alternatively-spliced mRNA isoforms. (**A**) Western blots comparing the effects of 72 hour DMSO (DM) or C16 treatment of MV4;11 (top) or MOLM13 (bottom) cells on levels of p53 and GAPDH (loading control). Representative images from three biological replicates are shown. Raw unprocessed gel images are presented in **Figure 6—source data 1**. (**B**) Differential alternative splicing events impacted by C6 (red) or C16 (blue) treatment of MV4;11 cells were quantified by rMATS. The number of significantly different events (> 5% $\Delta\psi$; FDR < 0.05) for each WIN site inhibitor are depicted in the graph. "RI" is retained intron; "MEX" is mutually exclusive exons; "A3SS" is alternative 3' splice site; "A5SS" is alternative 5' splice site; "SE" is skipped exon. See **Figure 6—source data 2** for output of rMATS analysis. (**C**) Sashimi plot quantifying read junctions that span exons 12–17 of *KRBA1* in MV4;11 cells treated with DMSO (green) or C16 (blue). Numbers in the arcs display junction depth. Skipped exon 15 is highlighted in orange. (**D**) As in (C) but for read junctions that span exons 20–22 of *TTF2*. Skipped exon 21 is highlighted in orange. (**E**) As in (C), but for read junctions that span exons 2 and 3 of *RPL22L1*. The location of exons 2 and 3 is depicted at the bottom. Splicing of exon 2 to the distal acceptor site in exon 3 results in an mRNA encoding RPL22L1a (orange); splicing to the proximal acceptor site in exon 3 results in an mRNA encoding RPL22L1b (yellow). (**F**) Left: Representation of amplicons used to discriminate between different *MDM4* (top) and *RPL22L1* (bottom) isoforms via semi-quantitative PCR. Right: Results of semi-quantitative PCR analysis for the various isoforms of *MDM4* and *RPL22L1,* and a *GAPDH* control, in MV4;11 or MOLM13 cells treated for 48 hours with DMSO or C16 (MV4;11, 100 nM; MOLM13, 250 nM; *n* = 3). All three biological replicates for DMSO and C16 are shown. Raw unprocessed gel images for the data in (F) are presented in **Figure 6—source data 3**. (**G**) Left: Representation of amplicons used to discriminate between *MDM4* (top) and *RPL22L1* (bottom) isoforms via RT-qPCR. Right: Results of RT-qPCR analysis for the various isoforms of *MDM4* (top) and *RPL22L1* (bottom) in MV4;11 or MOLM13 cells treated for 48 hours with DMSO or C16 (MV4;11, 100 nM; MOLM13, 250 nM; *n* = 3; Mean ± SEM). For each amplicon, isoform levels are expressed relative to the DMSO control. P-values are represented by asterisks: '*' ≤ 0.05, '**" ≤ 0.01, '***" ≤ 0.001.

Figure 6—figure supplement 2. Impact of RPL22 loss on the response of MLLr cells to WINi. (**A**) Western blot analysis of RPL22 expression in MV4;11, MOLM13, and K562 cells electroporated with Cas9 and either scrambled non-targeting (NT) control or *RPL22*-targeting sgRNAs. GAPDH and α-Actinin are loading controls. Representative images from three biological replicates shown. Raw unprocessed gel images are presented in **Figure 6—source data 4**. (**B**) GI_{50} values of C16 in NT and RPL22 KO MV4;11, MOLM13, and K562 cells in a 72 hour assay (*n* = 3; Mean ± SEM). (**C**) Number of genes with significantly (FDR < 0.05) altered transcript levels following treatment of RPL22 knock out (KO) or control (NT) cells treated with DMSO or 100 nM C16 for 48 hours, as determined by RNA-Seq (*n* = 4). See **Figure 6—source data 6** for complete output of RNA-Seq analysis. (**D**) Volcano plots, showing pairwise transcript level alterations in NT (control) and RPL22 KO MV4;11 cells treated 48 hours with DMSO or 100 nM C16 (red indicates FDR < 0.05). The location of transcripts from *ZMAT3* and *RPL22L1* are indicated. (**E**) Transcript level changes in WDR5-bound (left) and non-bound (right) RPGs in each of the indicated pairwise comparisons of RNA-Seq datasets. (**F**) Enrichment analysis of genes differentially induced by C16 in RPL22KO cells compared to control (NT) cells. KEGG and Hallmark.MSigDB pathways are shown. Fold enrichment of indicated pathways is presented on the x-

axis, the number of genes is shown in italics in each bar, and colors represent -Log10 FDR. See **Figure 6—source data 7** for complete enrichment analyses. (**G**) As in (F) but for suppressed genes. (**H**) Transcript level changes in mitochondrial ribosomal protein genes elicited by C16 in NT or RPL22KO cells.

Figure 6—figure supplement 3. Impact of RPL22 loss on the abundance of alternatively-spliced mRNA isoforms in MV4;11 cells. (**A**) Differential alternative splicing events affected by C16 treatment of control (NT) or RPL22 knockout (KO) MV4;11 cells were quantified by rMATS. The types of alternative splicing events are cartooned at left, and the number of significantly different events (> 5% $\Delta\psi$; FDR < 0.05) depicted in the graph. See **Figure 6—source data 8** for output of rMATS analysis. (**B**) Sashimi plot quantifying read junctions that span exons 5–7 of *MDM4* in NT or RPL22KO MV4;11 cells treated with DMSO or C16. Numbers in the arcs display junction depth. The location of exons 5, 6, and 7 is depicted at the bottom; skipped exon 6 is highlighted in orange. Note that RPL22KO images are also represented in **Figure 6F**. (**C**) As in (B) but for read junctions that span exons 2 and 3 of *RPL22L1*. The location of exons 2 and 3 is depicted at the bottom. Splicing of exon 2 to the distal acceptor site in exon 3 results in an mRNA encoding RPL22L1a (orange); splicing to the proximal acceptor site in exon 3 results in an mRNA encoding RPL22L1b (yellow).

Figure 1—figure supplement 1

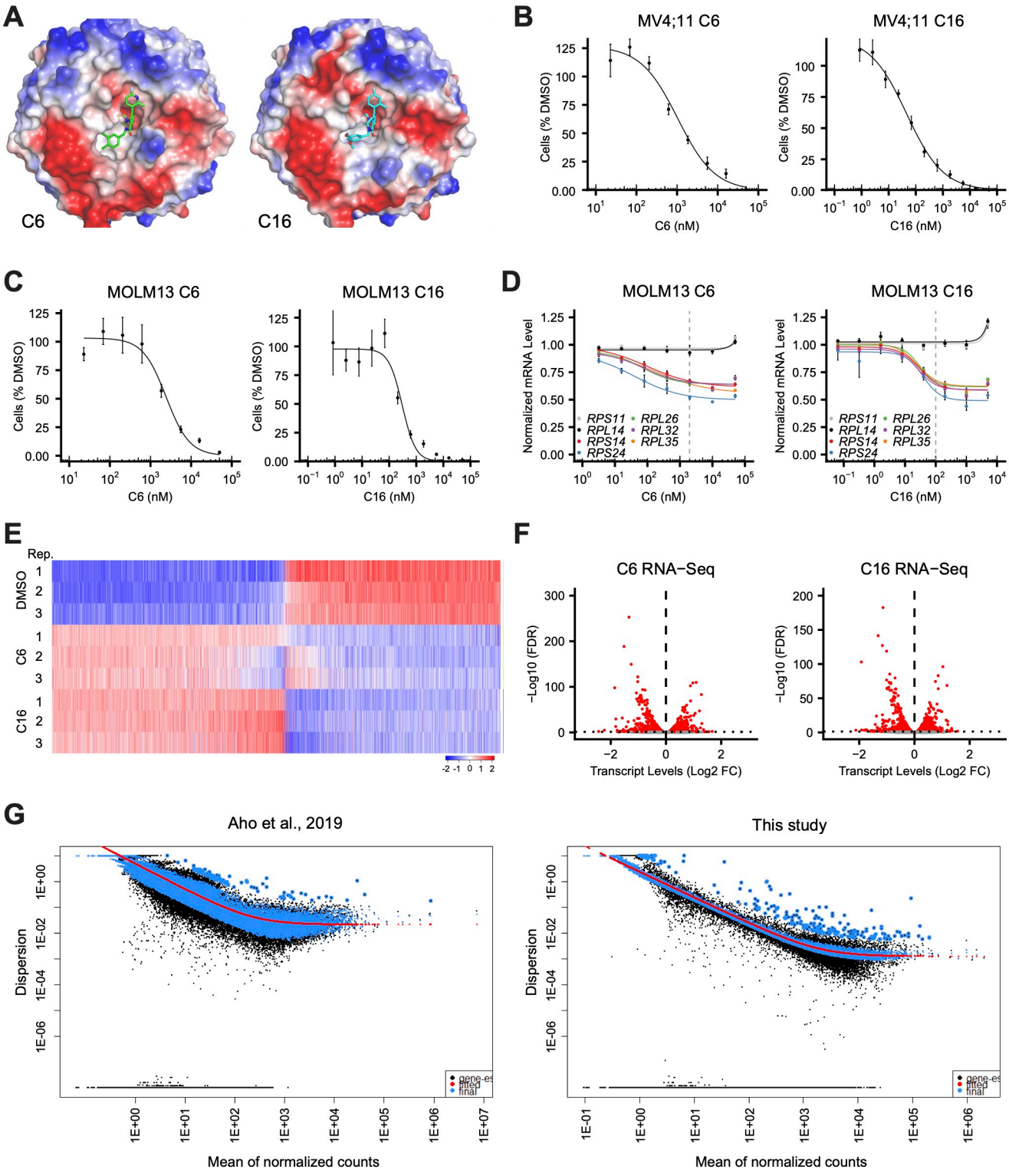

Figure 1—figure supplement 2

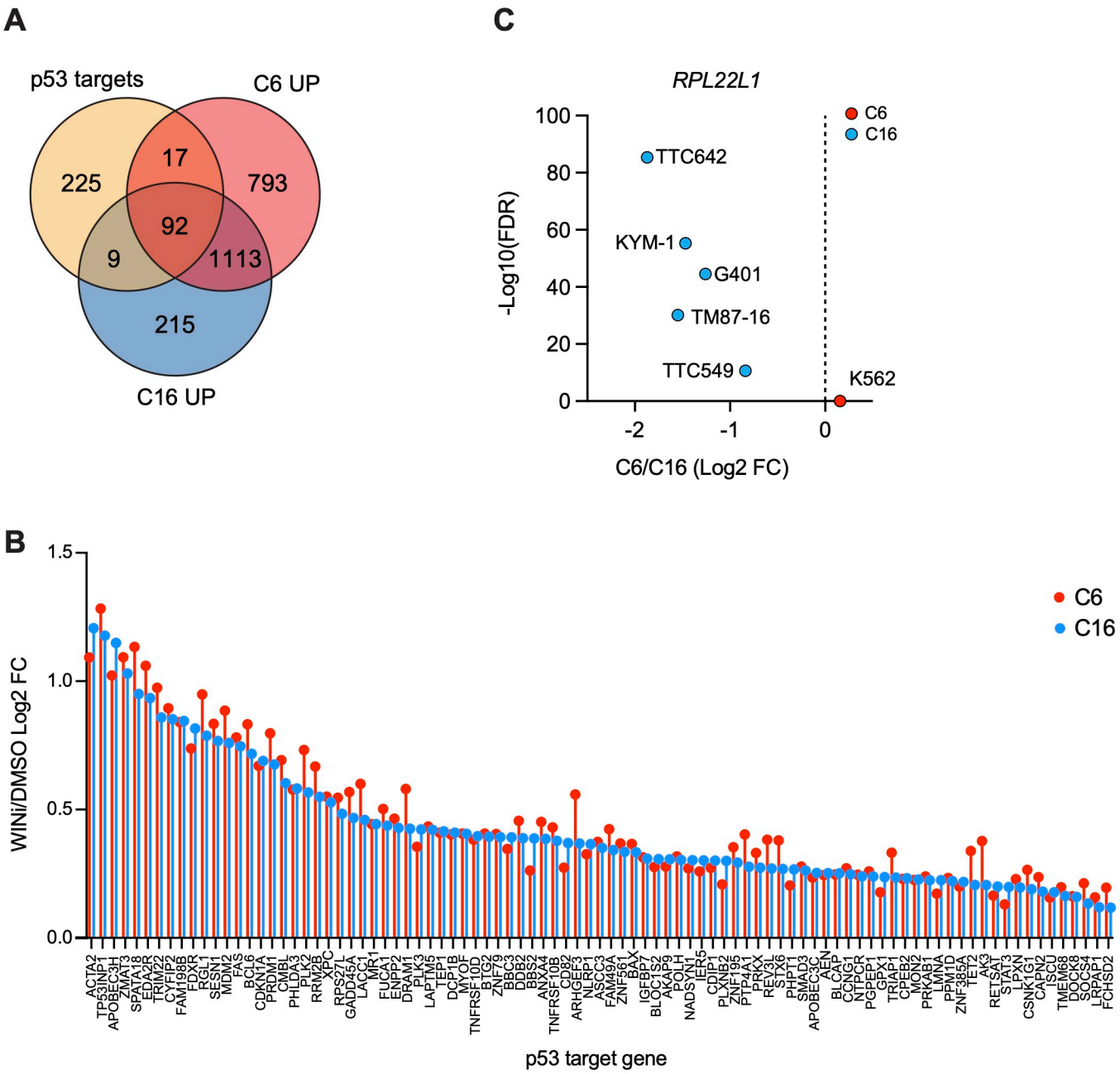

Figure 2—figure supplement 1

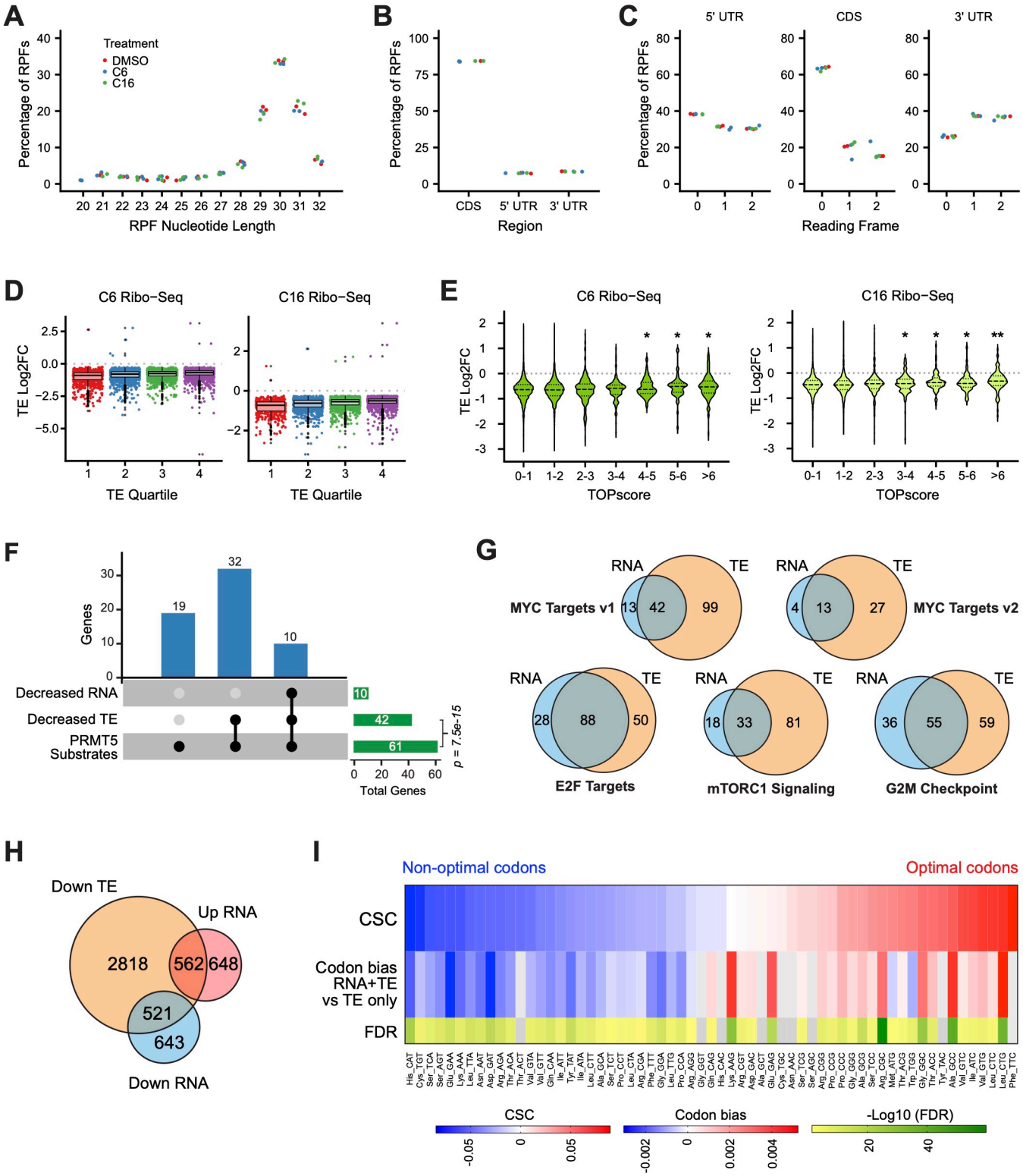

Figure 2—figure supplement 2

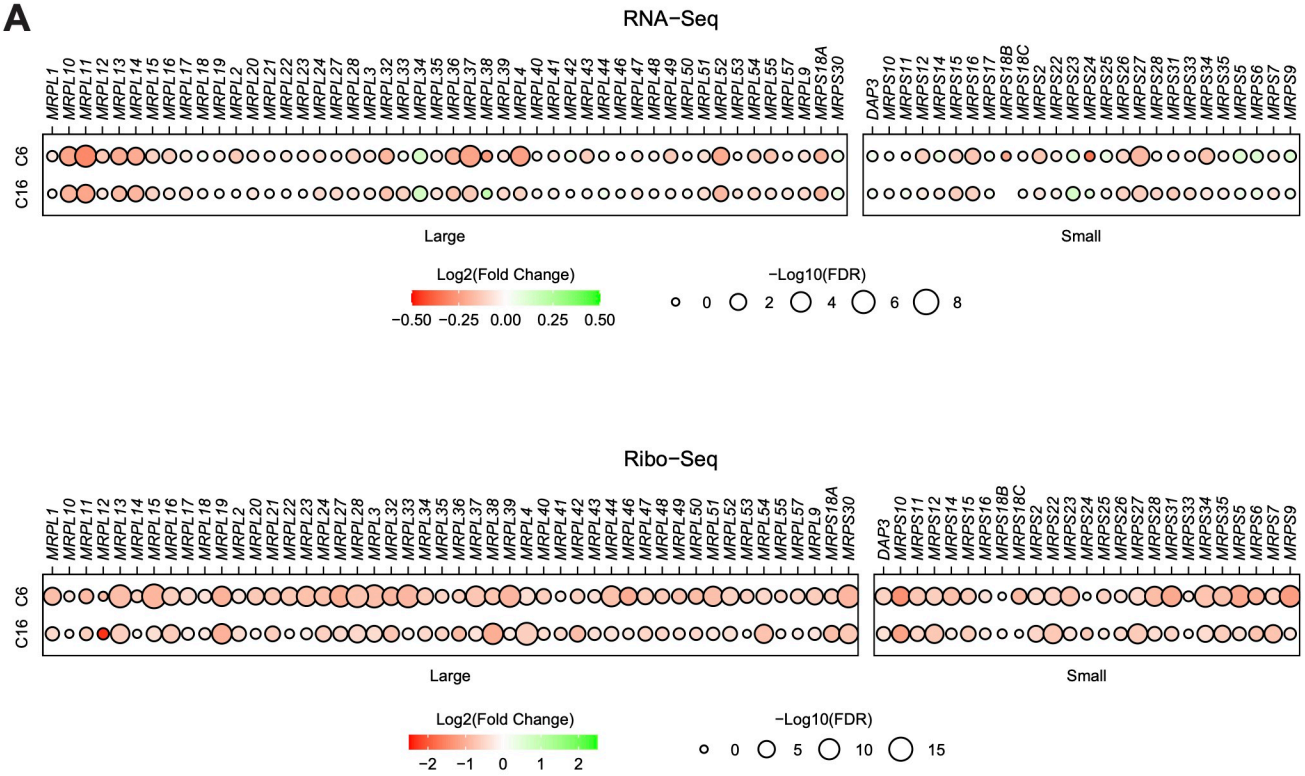

Figure 3—figure supplement 1

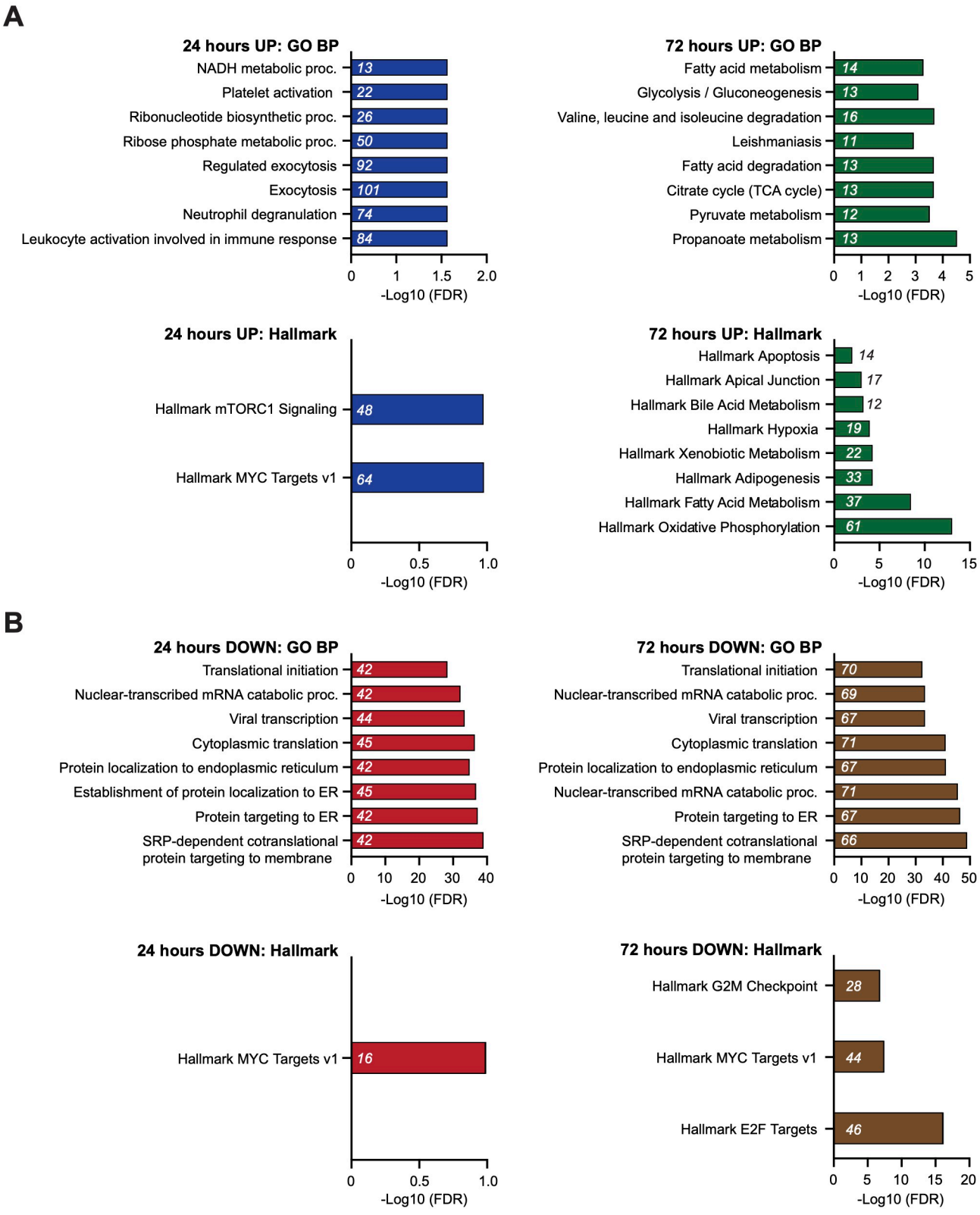

Figure 4—figure supplement 1

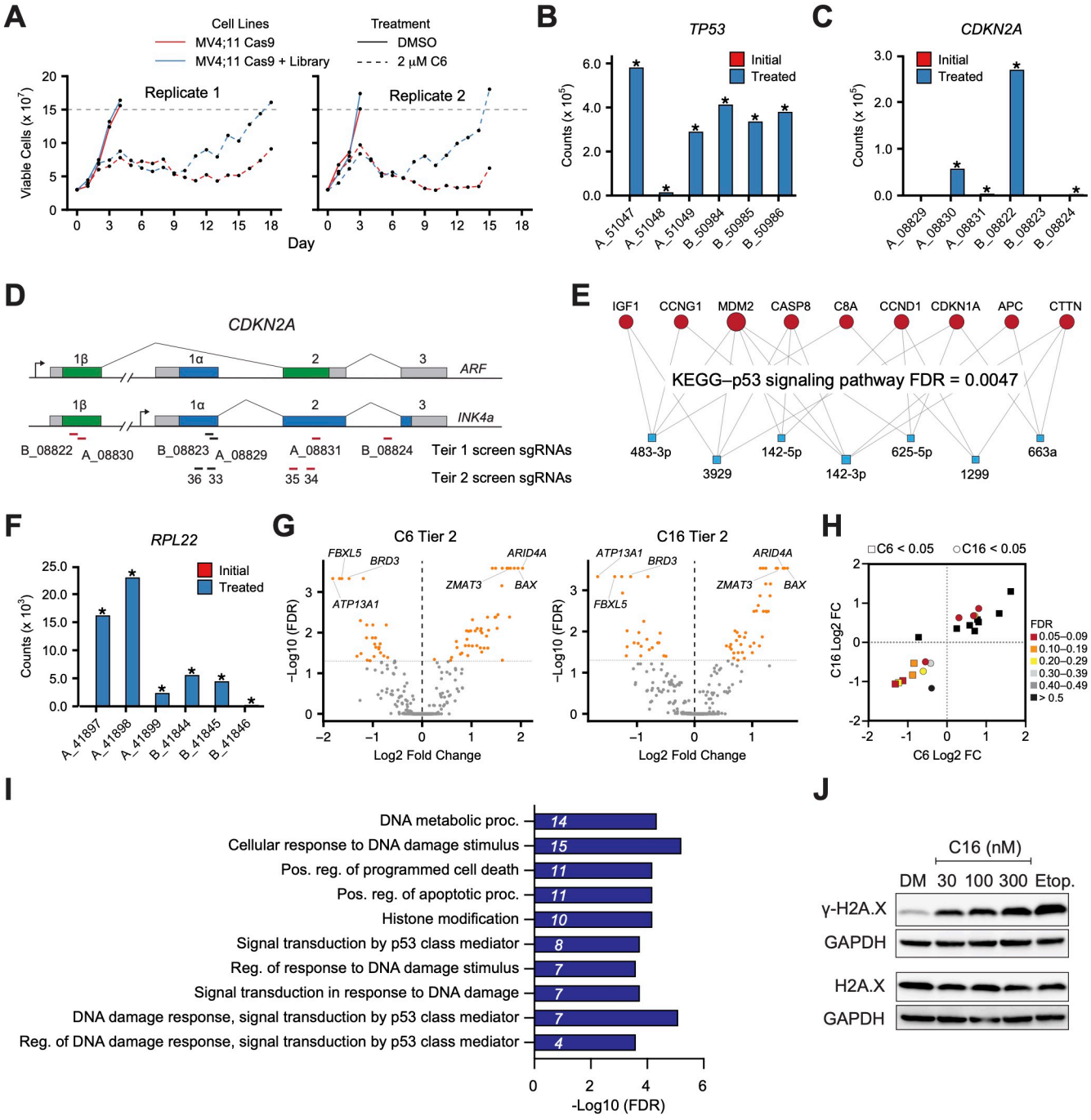

Figure 5—figure supplement 1

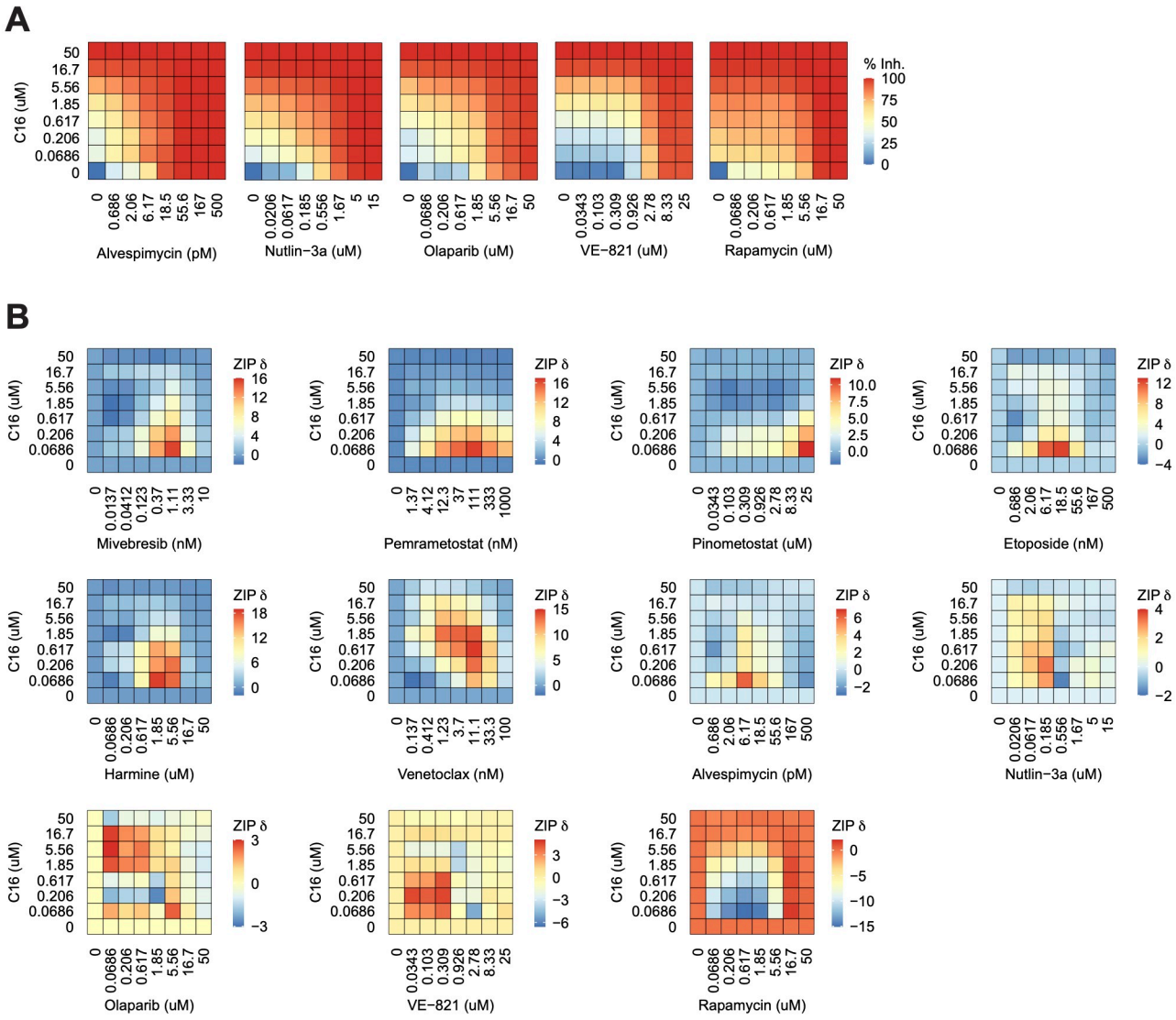

Figure 5—figure supplement 2

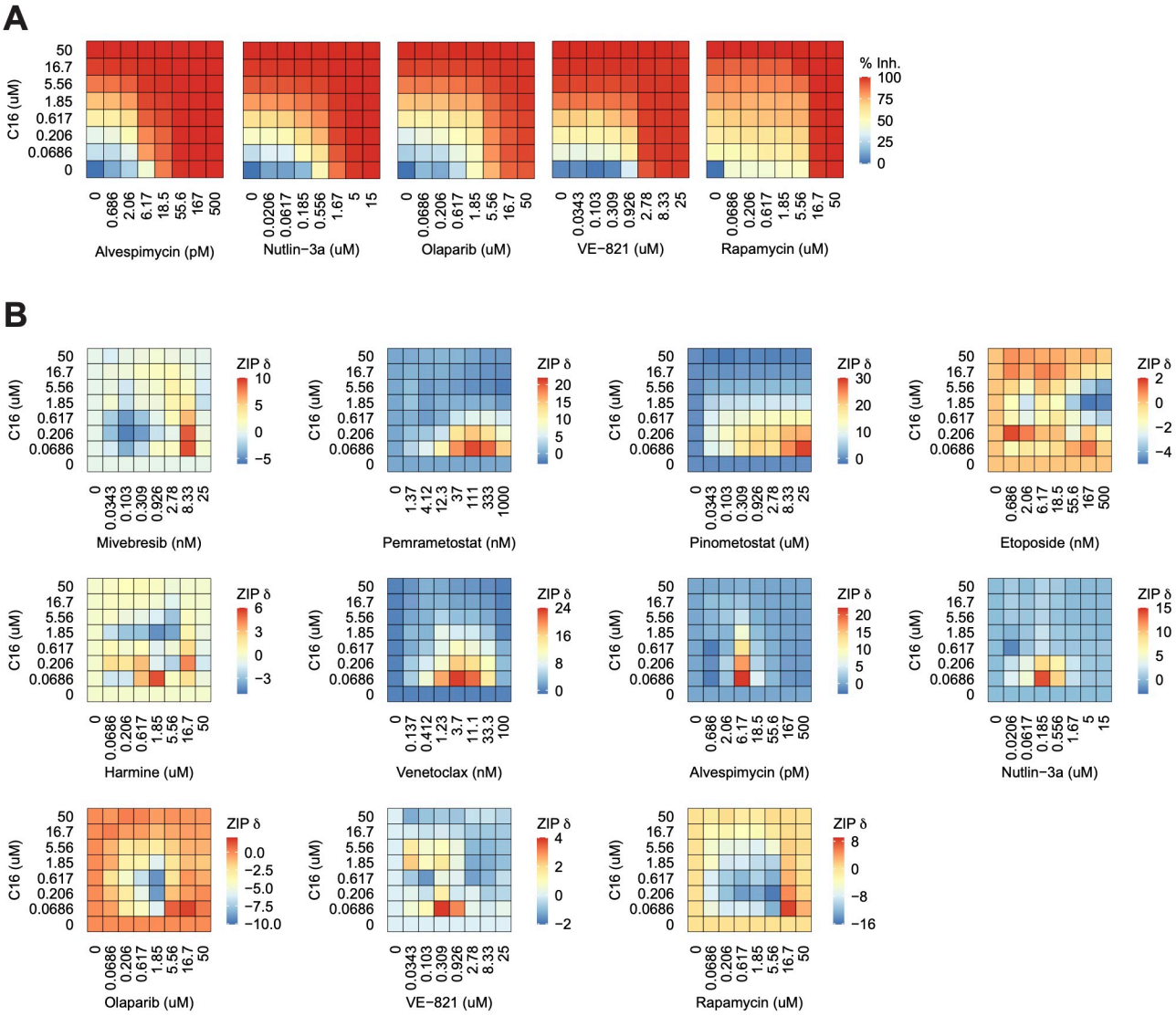

Figure 5—figure supplement 3

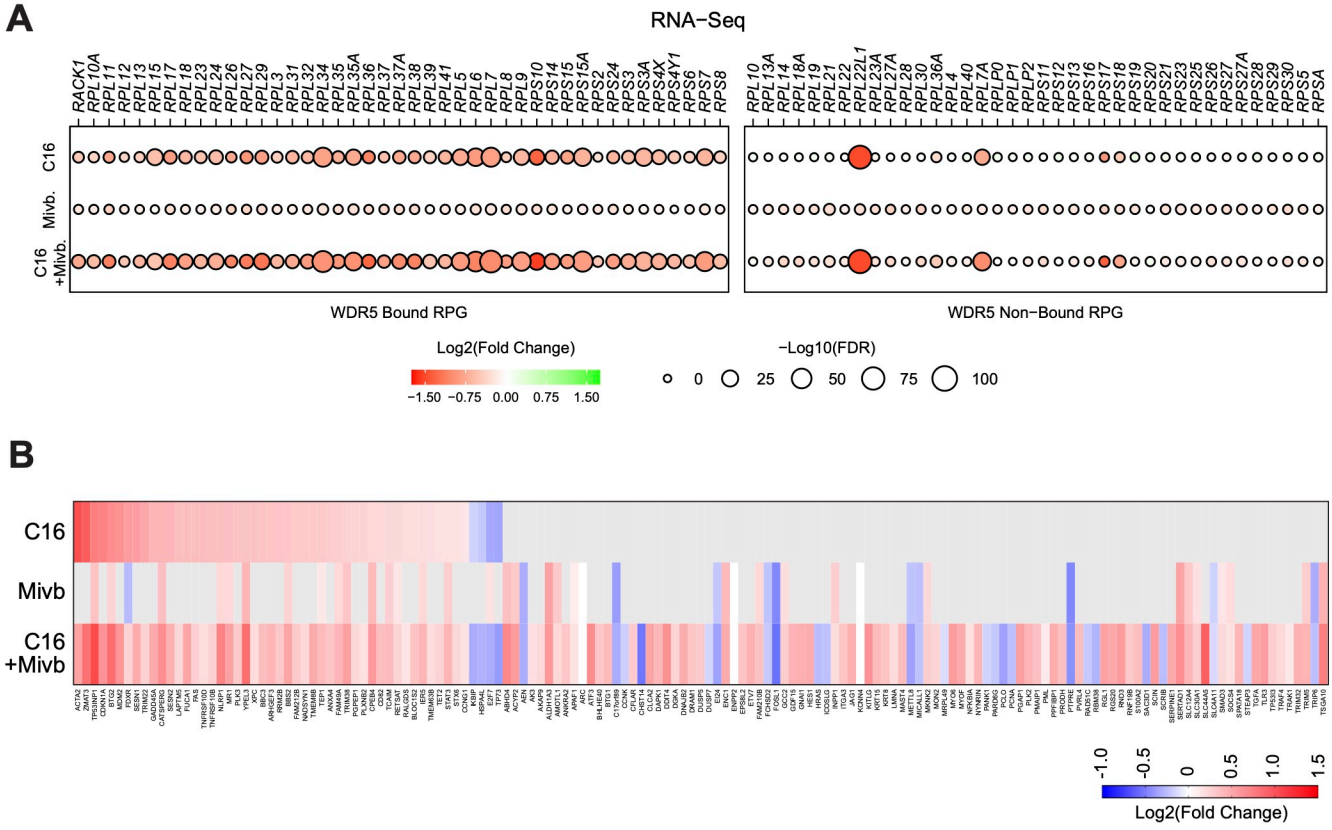

Figure 6—figure supplement 1

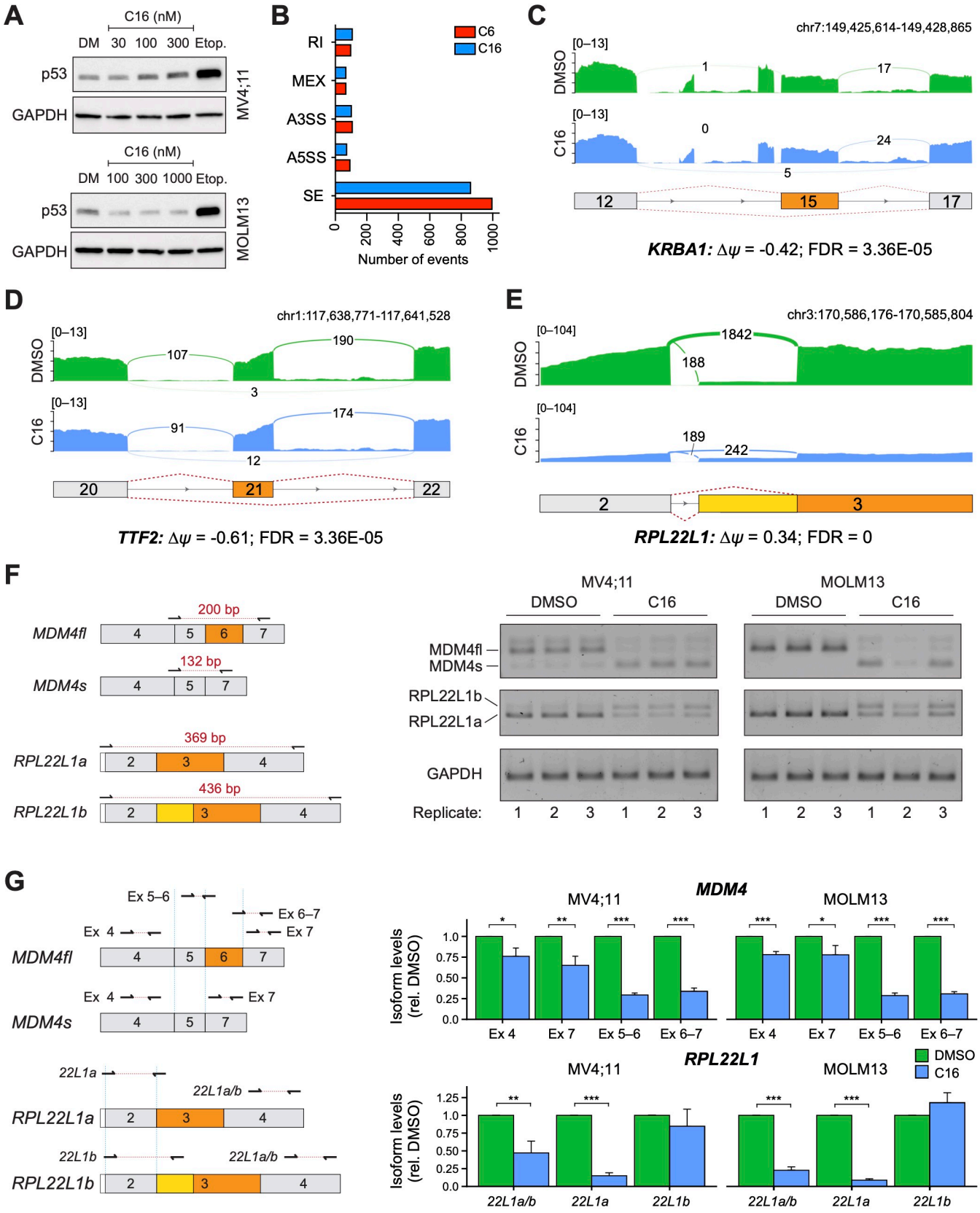

Figure 6—figure supplement 2

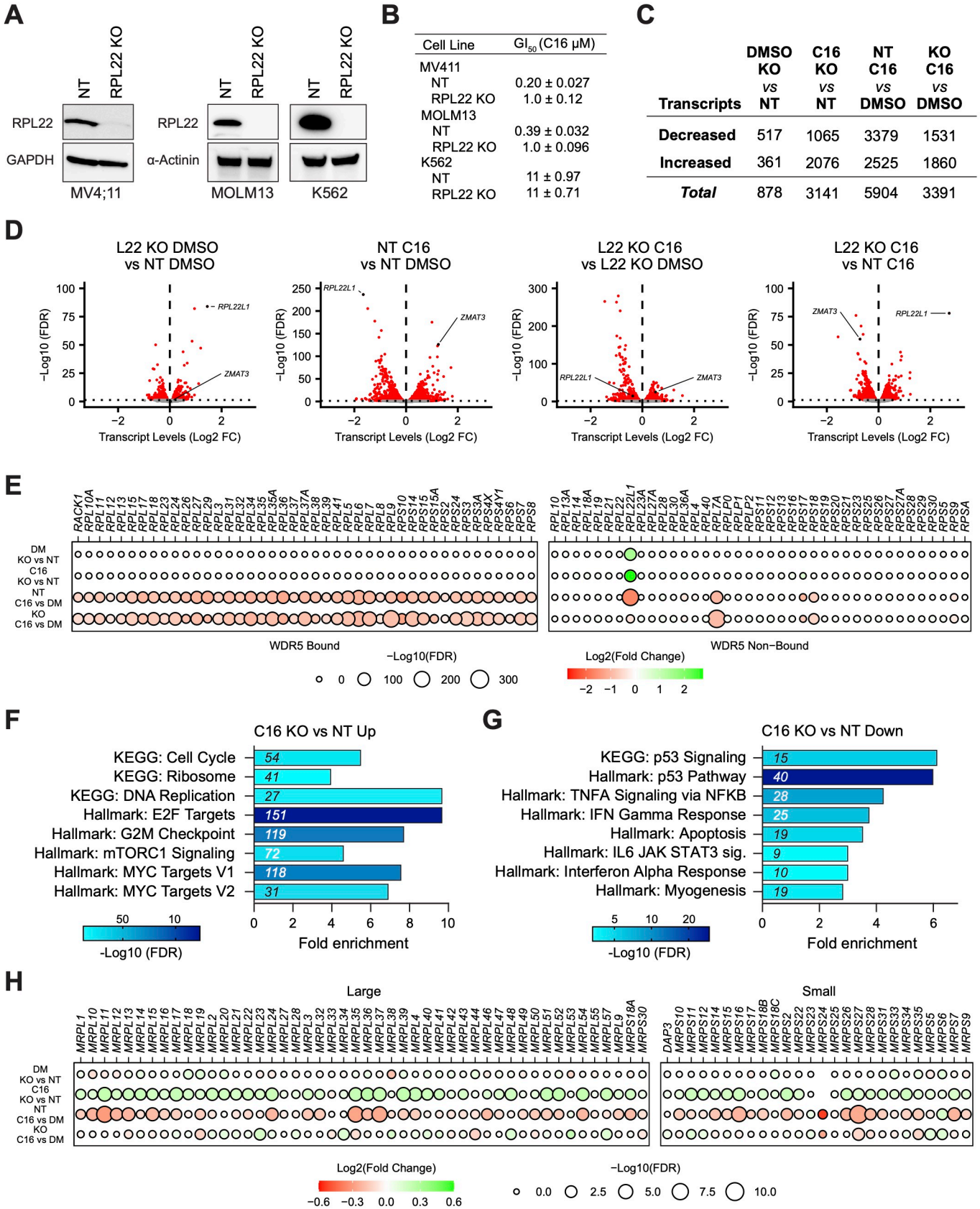

Figure 6—figure supplement 3